Nuclear Instruments and Methods in Physics Research A 1078 (2025) 170552

Contents lists available at ScienceDirect

Nuclear Inst. and Methods in Physics Research, A

journal homepage: www.elsevier.com/locate/nima

Full Length Article

Permanent magnet array with reduced stray field designed for a neutron supermirror polarizer

Earl Babcock [a,*], Olaf Holderer [a], Michael Monkenbusch [b], Dmitry Gorkov [c,d], Simon Staringer [a], Stefan Mattauch [a], Stefano Pasini [a], Helmut Soltner [e], Peter Böni [f], Markus Braden [c]

[a] Jülich Centre for Neutron Science at the Heinz Maier-Leibnitz Zentrum, Forschungszentrum Jülich GmbH, Lichtenbergstr. 1, 85748 Garching, Germany
[b] Jülich Centre for Neutron Science (JCNS-1) & Institute for Complex Systems (ICS-1), Forschungszentrum Jülich GmbH, 52425 Jülich, Germany
[c] II Physikalisches Institut, Universität zu Köln, Zülpicher Str. 77, 50937 Köln, Germany
[d] Heinz Maier-Leibnitz Zentrum (MLZ), Technische Universität München, Lichtenbergstr. 1, 85748 Garching, Germany
[e] Institute of Technology and Engineering (ITE), Forschungzentrum Jülich GmbH, 52425 Jülich, Germany
[f] Physik-Department, Technische Universität München, 85748 Garching, Germany

ARTICLE INFO

Keywords:
Neutron polarization
Supermirror
Magnetic yoke
Stray fields
Field compensation

ABSTRACT

We present a design of a permanent magnet (PM) assembly for a large volume that allows the reduction of long-range external stray fields through magnetic self compensation while also yielding a higher central field. The array described here was developed for a neutron polarization analyzer comprising a large-area supermirror (SM) array. The resulting array is self-compensated because it utilizes two groups of PM with equal but opposite dipole moments and involves modification to a permanent magnet based window-frame magnet. The principles of self compensation with permanent magnets presented are generally applicable for other applications where large volume magnetic fields with low stray field are required.

1. Introduction

Polarizing supermirror (SM) arrays for neutron polarization and neutron polarization analysis need to be magnetized in order to provide the desired performance [1], this is normally accomplished via permanent magnet arrays. These arrays commonly consist of rows of strong permanent magnets such as NdFeB arranged on either side of a cavity made of a pair of thick (≃ 1 cm) soft iron poles. Such dipole-like configurations can produce fields on the order of 50 mT (500 G) or more over the large volume of the SM array depending on its actual dimensions. However, these magnetic arrays, in addition to the desired central field of the cavity, create a large dipole field external to the device. Passive shielding with additional magnetic layers or shells of μ-metal, soft iron, or even steel, add much extra weight, complexity and size. Therefore we developed and produced a modification to the typical SM magnetic array to largely compensate the stray fields at long range. Adding anti-parallel magnets with the same but oppositely oriented total dipole moment suppresses the stray field at distances relevant to neutron instrumentation. The final device, shown in Fig. 1, is similar to a Halbach array and can be produced essentially as a "bolt-on" addition to existing polarized SM array magnetic arrays. Moreover, this modification also increases the magnetic field inside the assembly thus improving the magnetic saturation of the polarized SMs which in turn increases their neutron polarization performance.

For spin analysis of the scattered neutron beam the polarized cold neutron triple-axis spectrometer KOMPASS at the MLZ [2–4] was recently equipped with a high-performance multichannel polarizing V-cavity consisting of a large-area spin analyzing SM array for its secondary spectrometer. The outer dimensions of this spin-analyzer assembly are 122 mm × 238 mm in cross-section and 645 mm in length consisting of the casing with the SM spin analyzer within a PM version of a window-frame magnet cavity. Window-frame magnets are broadly used in accelerator physics and commonly utilize resistive or superconducting field coils on "yokes", rather than the permanent magnets used at KOMPASS [5,6]. At KOMPASS this magnetic cavity is made with rows of permanent NdFeB magnets on either side separating a pair of thick soft iron plates that act as magnet poles creating a dipole field with an air gap. Such an array provides a permanent saturating field ensuring high neutron polarization efficiency of the SMs that form the V-cavity [7]. The magnetic cavity creates a large field of about 65 mT (650 G) inside its volume but also a corresponding large dipole field outside of it. Because a neutron triple-axis spectrometer measurement involves scanning three angles, the angle of the primary spectrometer

* Corresponding author.
E-mail address: e.babcock@fz-juelich.de (E. Babcock).

https://doi.org/10.1016/j.nima.2025.170552
Received 25 October 2024; Received in revised form 4 April 2025; Accepted 20 April 2025
Available online 5 May 2025

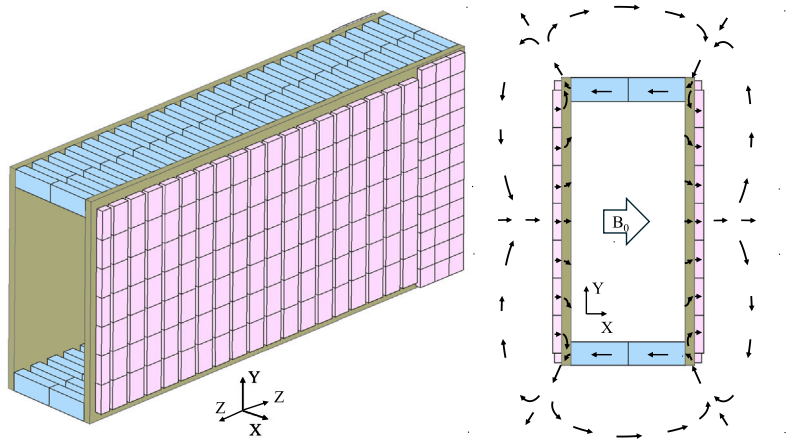

Fig. 1. A drawing of the novel PM array, showing a 3D model on the left hand side and the cross section on the right hand side with the magnetic flux pattern indicated with arrows. The olive green slabs represent the thick iron plates used for poles, and the parts colored in blue and pink represent NdFeB magnets with magnetization to the left and right respectively. The central magnetic field, B_0, points to the right as indicated. This arrangement yields a uniform inner field that resembles a sextuple externally.

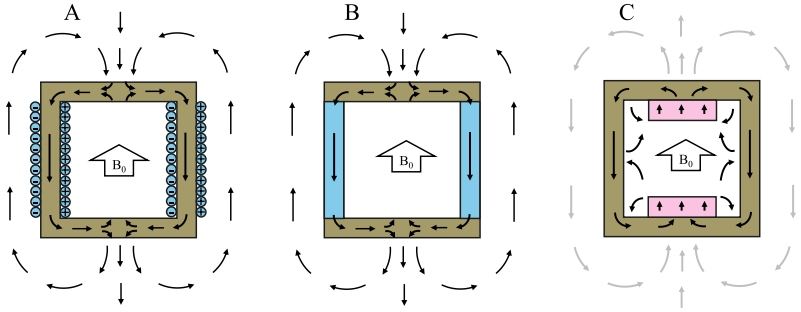

Fig. 2. Diagrams of the magnet cavities described in the text. In the figure, olive green is iron, blue are wires or PM that create a magnetic flux downwards and pink are PM with upward flux as indicated. A is the common window frame magnet magnetized by the indicated current-sheet coils. B is the PM equivalent of the window frame magnet which uses stacks of magnets to mimic the magnetization profile of A. C is an air-gapped permanent magnet cavity that uses an iron tunnel as a yoke. While the yoke makes a closed flux-path, the active uniform volume is smaller than in A or B. The flux lines of C are like an iron-pole Halbach array (diagram 13.6 (b) and (e) from [8]) but are magnetically much different to A and B which have a nearly full usable cross section but make a dipole field externally.

for neutron energy selection (first axis), the take-off angle of scattering from a sample (second axis), and the secondary spectrometer detector arm to determine final neutron energy (third axis), a complex movement pattern is created. Therefore the stray field of the PM cavity, mounted on the secondary spectrometer, will cause a time variation in the ambient magnetic field around it.

The KOMPASS triple-axis neutron spectrometer is installed next to the Jülich Neutron Spin Echo (J-NSE) spectrometer [9], another polarized neutron instrument which is highly sensitive to magnetic field gradients and/or time instabilities in the magnetic field environment along its entire neutron flight path. A typical NSE experiment measures quasielastic and inelastic scattering from soft-matter samples at a series of scattering vectors (**Q**). The scattering can be weak which requires many days of data collection under stable magnetic field conditions. During commissioning and initial use of the KOMPASS spin analyzer, variations of the magnetic field at the location of the J-NSE neutron flight path on the order of few μT (tenths of mG) were caused by the detector arm movements. This undesired cross-talk to the J-NSE greatly limited its user operation. However, with the data we were able to quantify the magnitude of the magnetic cross-talk to the J-NSE by both magnetic field sensors and also the shift in the neutron spin-echo pattern which in itself acts as a high-precision magnetometer. Additionally reduction of stray magnetic fields is also important for the optimal function of the KOMPASS instrument as interference with its own magnetic guide fields can severely reduce the precision of the neutron polarization analysis.

A solution to allow the free and simultaneous operation of both KOMPASS and J-NSE with high precision was required. Shielding options on the KOMPASS instrument were briefly considered, but would have required large modifications to its detector arm. Passive magnetic shielding has been employed for a similar NSE instrument at SNS to prevent similar effects but this requires significant space [10]. An active shielding option of the J-NSE itself was considered but has been discontinued for the time due to the high costs and efforts needed [11]. Up to now the only readily feasible solution has been to employ self compensation in the magnetic casing design of casing for the SM spin-analyzer array, namely a type of Halbach configuration.

2. Magnetic design

In general two simple types of dipole arrangements with soft-iron/high-permeability elements can be made. The first example, as used in the original KOMPASS array, is where the magnets are arranged in columns above and below the beam axis using the iron elements on the N and S poles as pole shoes to guide the horizontal field which is the permanent magnet analog to the electro-magnet shown in Fig. 2A and B respectively, which are commonly referred to as window frame magnets [5,6]. The second type is an iron tunnel where magnets of the same magnetization direction are attached to the inside upper and lower caps of the tunnel. Here the air-gap flux is from the N pole of the lower magnet(s) to the S pole of the upper magnet(s) with the return flux going around either side of the tunnel which then acts as a magnetic yoke, see diagram C in Fig. 2 [8]. Each tunnel of these types then has a rectangular cross section that can be varied. Example C, being fully yoked in the transverse plane, has a much suppressed external field compared to the long-range dipole-like field of A, and B.

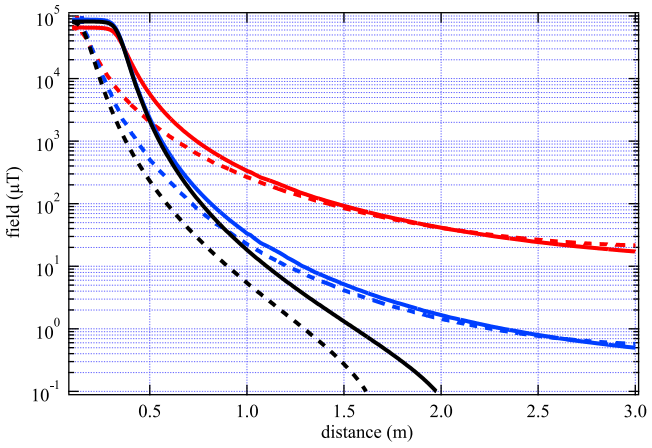

Fig. 3. Plots of the calculated field magnitude of the old dipole-like array (red), the new Halbach-type array as built (blue) and the Halbach-type array with theoretical maximum stray field compensation (black) for the longitudinal direction which is parallel to the neutron beam and along its 65 cm length (solid lines) and the transverse direction which is perpendicular to the neutron beam (dotted lines). At the closest distance, the KOMPASS PM array can be ca. 2.5 m from the NSE neutron path.

We note that a cylindrical-geometry Halbach array is a PM arrangement such that, $\mathbf{M}(\theta) = M_0(\sin([k+1]\theta)), (\cos([k+1]\theta))$ with θ the angular position of the origin of the dipole moment of a discrete magnet from the y-axis, where a typical Halbach cylinder with radial symmetry is assumed, and $k = 1$ yields an internal uniform field and vanishing external field for continuously varying magnetization [12,13]. In the references n is used to signify the number of the current-sheet equivalent permanent magnets or iron-core electromagnets [14]. For discrete block-type magnets, *i.e.* low n, the external field will not be 0, but rather a multiple related to n. In this description 2 A and B would be like a $k = 1$ Halbach with $n = 2$ and iron poles.

The external stray-field compensation we employed involves beginning with a PM window-frame cavity as in Fig. 2B and adding NdFeB permanent magnets of equal magnetic moment to those of the existing ones, but with their magnetization in the opposite direction. These additional magnets are mounted onto the outer surface of the soft iron pole plates of the original array. This arrangement looks similar to a simplified cladded magnet [15] which is another variation of a $k = 1$ Halbach array, now with $n = 4$ current sheet equivalent magnets. This particular Halbach geometry with $n = 4$ yields a rather high field homogeneity in the entire volume [14]. In addition the iron pole plates homogenize the field in the longitudinal direction (i.e along the beam direction) as in [16]. However, here we make two additional modifications, the aspect-ratio of height-width is not 1, and the magnets from the original split-dipole arrangement must not make continuous and discrete frames with the additional magnets added onto the iron pole plates.

Such a Halbach-like arrangement has two advantages for this particular application. First, ensuring equal total magnetic moment for the opposite permanent magnets suppresses the long-range dipole field, and, second, the additional magnetization actually increases the internal field of the array compared to the original dipole by about 30%. On the one hand, using a higher field for the magnetization of the SM should improve the neutron polarization efficiency and lower any remaining diffuse magnetic scattering [1]. On the other hand, if one were to accept the original 0.055 T field as in the original dipole arrangement, one could reduce the magnet density in the Halbach-type magnet design by approximately 30% which would be observed as a proportional further reduction in the stray field.

Results of finite-element method (FEM) calculations of the old dipole-like and of the Halbach-type magnet arrays are shown in Fig. 3. A conceptual diagram of the new array is shown in Fig. 1. The Halbach-like design indeed produces a flux pattern very similar to an $n = 4$ Halbach, but stretched to the rectangular geometry. This type of array produces an external sextupole field as a dominant term and the resulting magnetization patterns in the material are much different than the examples shown in Fig. 2.

In accelerator physics, the quality of such an array is often quantified by looking at the form of its magnetic moment contributions which can be represented as a Fourier series of the contributing moments, i.e. dipole, quadrupole, sextupole etc. about a given radius where an ideal/balanced configuration would produce close to a single contribution to the series, see chapter 6 of [17] for example. While such an analysis is normally performed with respect to the active volume of a magnetic arrangement, arguments given in [17] can be extended to represent the field outside the system. When one can assume a simple radial symmetry, i.e. infinite length the problem reduces to a 2D analysis. The radial field at a given radius outside the magnet can be represented by a Fourier series of the form

$$B_r(r,\theta) = \sum_i B_i \sin(i\theta) + A_i \cos(i\theta) \tag{1}$$

where B_i and A_i are the normal and skew multipole coefficients, respectively, and i an integer. The perpendicular components $B_\phi(r,\theta)$ can also be represented with a similar series. If the multipole moments are oriented along $\theta = \pi/2$ then the A_i coefficients are zero.

For the simplified 2D version of our Halbach-like array one can determine the series representing the dipole contributions from the field along a simple circle. Results shown in Fig. 4 are the results for an example array with a separation of the iron plates, h, equal to double their width, w, where we plot the results at radius $r = h$ on the left hand side, and at multiples of r/h on the right hand side. For the 2D case the long-range fields scale as $B_i^{2D} \propto 1/r^{i+1}$. This geometry is very well described by the first 3 allowed terms, $i = 1, 3, 5$. For the compensated Halbach-like array with the multipole moments oriented along $\theta = \pi/2$ fits to Eq. (1) yield $B_3 \simeq 19.4 \times B_1$ and $B_5 \simeq -4.4 \times B_1$ at a radius $r = h$ showing a dominant $i = 3$ sextuple and $i = 5$ decapole moment. For comparison, also on the left hand side is an uncompensated array of the same size. Here the fits to Eq. (1) yield $B_3 \simeq -B_1/3$ and $B_5 \simeq B_1/20$ showing that the $i = 1$ dipole term is dominant and is 24 times larger with opposite sign compared to the compensated Halbach-like array.

For the compensated case, even though the decapole and sextupole terms replace the dipole term and dominate at short distances, the long-range field is still given by the remaining diminished dipole contribution. The various multipole terms result from the extended geometry and symmetry of the PMs so they cannot be individually eliminated. In the full 3D simulation shown in Fig. 3 comparison of the magnitude of the long-range field for the compensated and uncompensated case implies a ca. 100 fold reduction is obtainable for ideal balancing of magnetic moments of the PMs for the actual geometry of the KOMPASS analyzer PM array.

3. Mechanical design and construction

Care must be taken to design the static mechanical system as arrays of this type store a significant amount of mechanical energy. In the new design, there is now a repulsive force of about 7000 Newtons between the iron plates, which are clamped in place against this force via bolts through the iron poles to the (pre-existing) aluminium support fixing the placement of magnet columns between the iron plates. The additional magnets placed on the iron plates have an attractive force to the iron plate, but the forces between the neighboring magnets are from 1 to 10 Newtons and repulsive except for the rows on the edges which experience higher repulsive forces from 10 to 20 Newtons. Therefore, a slotted aluminium cap plate with set screws on the ends of the slots is used on top of these magnets to hold them in place. The individual groups of magnets between the iron plates and those added onto the iron plates do not have identical dimensions. Since the iron plates and

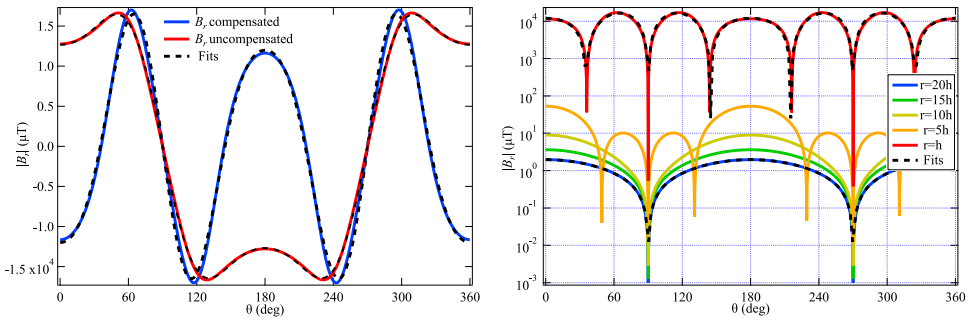

Fig. 4. Plots of the radial field values, B_r of a $h = 2w$ self compensated array (blue) and uncompensated array (red) from 2D FEM simulations. On the left hand side is B_r at $r = h$ and on the right hand side is the absolute value of B_r at multiples of r/h for an ideally compensated array with matched total dipole moments of the two PM groups. The dashed black lines are fits to Eq. (1).

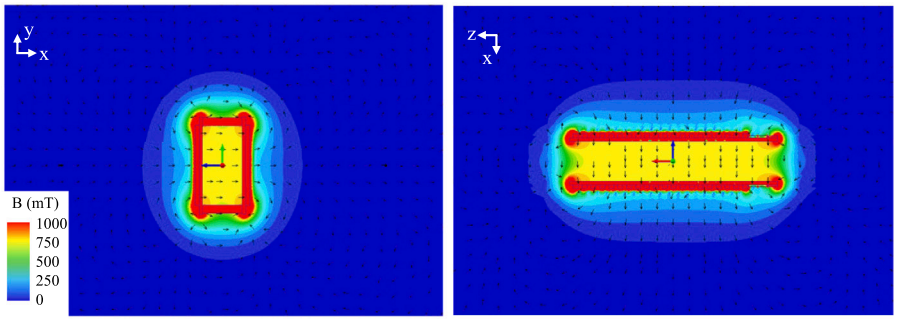

Fig. 5. FEM calulations of the new compensated array. The left hand side shows the field in the XY vertical plane, and the right hand side shows the XZ plane as defined in Fig. 1. The flux arrows show the sextupole form of the resulting field on the 2D symmetry planes. Note the rotated orientation of this diagram compared to Fig. 2 corresponding to the orientation of our actual array shown in Fig. 1.

magnet are of similar thickness, the iron remains below saturation with a high slope in relative permeability (the iron relative permeability goes close to 1 at $\simeq$ 1.6 T, whereas the saturation magnetization of NdFeB magnets is ca. 1.2 T) so they effectively homogenize the magnetic flux. Consequently, a moderately non-uniform arrangement of the magnets on the iron plates should not largely affect the field or uniformity of the inner volume. The number of magnet pillars between the iron plates need not be equal to the number of rows on the iron plates provided that both are arranged uniformly enough to prevent local saturation of the iron plates and that the total magnetic moments of the two groups are balanced (see Fig. 5). Using these principles, the actual array as shown in Fig. 1 was built. The magnetic pillars, their slotted aluminium support structure, and the iron plates were not modified other than the addition of some mounting holes in the iron poles and aluminium support to secure the new aluminium slotted cap plates and to clamp the iron poles in place.

In the first revision of this particular array there are 23 evenly spaced original magnet pillars on either side between the 10 mm thick 306 mm high by 655 mm long soft iron plates. Each of these 46 pillars consist of 2 PMs of the size $62.0 \times 25.0 \times 16.0$ mm^3, colored blue in Fig. 1. There are 22 additional rows of PMs on the Fe plates, colored pink in Fig. 1. most of which consist of 7 pieces of $10.0 \times 40.0 \times 20.0$ mm^3 except for the first row on one edge which consists of 7 PMs of $10.0 \times 40.0 \times 15$ mm^3 and the last three rows from the other side which consist of 12 PMs $8.0 \times 25.0 \times 25.0$ mm^3 in size. This arrangement for the new rows of magnets on the iron plates was chosen to accommodate other existing mechanical structures such as biological shielding around the casing and to be able to use standard commercially available magnet dimensions. Using these dimensions the two groups of magnets would have a ca. 8% mismatch, which can be improved. Furthermore we expect empirical adjustment of the magnet volumes are required to achieve optimal compensation in real instances.

A drawing of this new Halbach-type magnet structure is shown in Fig. 1. Here we point out a few important features. The magnets are placed in rows with some separation between them. A gap is important as it prevents excessive repulsive forces between the magnet rows, and it enables variation of the magnet sizes to balance the dipole moments of the two magnet groups using commercially available magnet dimensions. Further there are aluminium supports structures (not shown) around both the magnet rows and columns to hold them in place against the moderate forces between the magnets which also serve as a clamp to hold the iron plates in place against the larger net repulsive force of the assembled array.

4. Test experiments and comparison

Tests of the "isolated" arrays measured with a high-sensitivity Hall probe which can be compared to the FEM calculations as well as tests of the interaction/cross talk of this array as seen by the J-NSE instrument were performed. Fig. 6 presents Hall probe measurements away from the neutron instrument which indeed show a large reduction in the stray fields already at a distance of 1.5 m, but the accuracy of this reduction is near the sensing limits of the Hall probe used [18]. The 8% mismatch of the new compensating PM magnetic moments leads to about a 25 x reduction in stray field at 3 m distance as in the calculated fields shown in Fig. 3, but the measured fields of the actual arrays fall off faster than the FEM calculated fields do. This is probably because the FEM calculation was conducted for a system in an ideal non-magnetic surrounding whereas the actual system was in a building with various steel elements around it, which serve as magnetic conductors to pull the flux away from the array faster than in the relative permeability $\mu_r = 1$ bounding volume of the calculation.

For a practical comparison, a reference position of the upstream J-NSE $\pi/2$ flipper position which is at the beginning of the J-NSE instrument and the closest point to the KOMPASS analyzer array was chosen. This location is around 2.5 m to 4 m away from the KOMPASS detector arm depending on its placement. The FEM calculated values for the uncompensated system vary by about 13 μT (130 mG) whereas

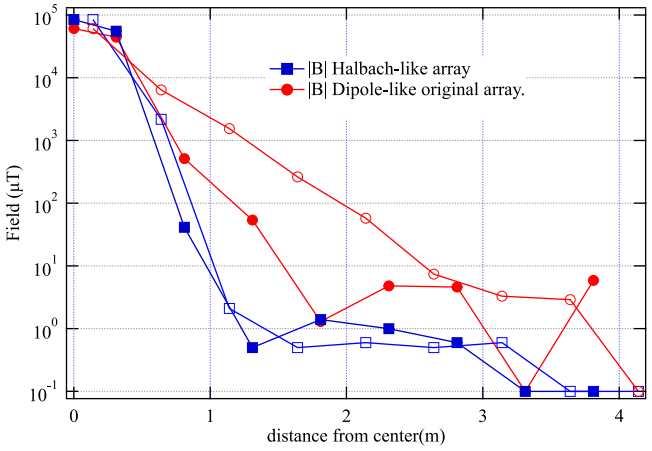

Fig. 6. Graph of the measured fields for both the old dipole-like design (red) and the new Halbach-type magnet design (blue) corrected for the ambient field. Closed markers are for the Z direction i.e. longitudinal to the tunnel of the array and open markers are for the X direction, i.e. transverse. The lines are to guide the eye. At the larger distances the values are near the sensitivity limit of the Hall probe we used.

with the new system they are more than 25 times less, *i.e.* a 0.5 μT variation between 2.5 m and 4 m distances. These calculated field variations for the uncompensated array are actually about 4 times higher than measurements with the 3-axis Hall probe on the J-NSE instrument itself for the uncompensated array which gave a change of 3.5 μT (35 mG) upon movement of the KOMPASS detector arm. However, for the compensated array the 0.7 μT (7 mG) difference measured upon scanning of the detector arm from the 2.5 m to 4 m distance from the J-NSE reference position and back is in agreement with the FEM calculations. Therefore a fivefold reduction in the relative disturbance is obtained between these positions vs. the factor of 25 predicted in the FEM calculations for the as-built case. With further balancing of the actual array we expect a further reduction of the relative disturbances at the J-NSE reference position of up to a factor of 10 more than presently achieved. The lower than predicted relative disturbance from the un-compensated array in these practical conditions is likely again due to coupling of return flux-paths through nearby iron or steel instrument components (i.e. with $\mu_r \gg 1$) preferentially influencing the dipole portion of the resulting flux pattern which is the dominant portion for the uncompensated array.

5. Conclusions

With a straight-forward application of self-compensation, using this Halbach-like magnetic arrangement we have developed and verified a method to reduce long-range stray fields of permanent magnet arrays. For our particular application, relative disturbances from the stray fields from the KOMPASS analyzer at the position of the J-NSE upstream $\pi/2$ flipper (closest point) have been reduced by more than a factor of 5. Fine turning of the balance of magnetic moments can further improve this result. Clearly the idea of active self-compensation has been widely used in electromagnet design, especially for high-field superconducting magnets which would be difficult to passively shield. Here we show the same sort of principles can be used to reduce stray fields and cross-talk from PM arrays. Typical self-compensated electromagnet arrays, such as compensated split-pair magnets, use opposing dipoles of different size but equal dipole moments resulting in a reduced magnetic field for the active volume. In contrast, for the methods presented here, using PM's with equal but opposite dipole total moments and iron pole pieces, the magnetic field inside the active region is increased while maintaining the advantages of self-compensation, namely reduced stray fields and magnetic coupling. Thus, the type of self-compensated permanent magnet array based on a Halbach magnet design provides multiple advantages for applications while known downsides are comparatively minor and technical in nature. Such known downsides are limited to added assembly time and the slight increase in cost where the cost of the magnets and the mechanical assembly is typically only a few percent or less of the total cost of the instrumentation using such magnetic arrays. Based on our experiences with schemes for passive shielding or active compensation, the solution presented here is extremely cost effective, and better performing. We would encourage such design principles to be utilized whenever possible.

CRediT authorship contribution statement

Earl Babcock: Writing – review & editing, Writing – original draft, Methodology, Conceptualization. **Olaf Holderer:** Writing – review & editing, Resources, Methodology, Investigation. **Michael Monkenbusch:** Writing – review & editing, Methodology, Investigation. **Dmitry Gorkov:** Writing – review & editing, Resources, Methodology, Investigation, Conceptualization. **Simon Staringer:** Investigation, Conceptualization. **Stefan Mattauch:** Writing – review & editing, Project administration, Funding acquisition. **Stefano Pasini:** Writing – review & editing, Resources, Project administration, Investigation, Conceptualization. **Helmut Soltner:** Writing – review & editing, Investigation, Formal analysis, Conceptualization. **Peter Böni:** Writing – review & editing, Methodology. **Markus Braden:** Writing – review & editing, Project administration, Methodology, Funding acquisition, Conceptualization.

Declaration of competing interest

The authors declare the following financial interests/personal relationships which may be considered as potential competing interests: Peter Boeni reports a relationship with Swiss Neutronics that includes: board membership, employment, and equity or stocks, However, this relationship does not involve any competing financial interests or personal relationships that could have influenced the work reported in this paper. Other authors declare that they have no known competing financial interests or personal relationships that could have appeared to influence the work reported in this paper.

Acknowledgment

We acknowledge funding by the BMBF through the ErumPro project 05K19PK1.

Data availability

Data will be made available on request.

References

[1] C Klauser, Th. Bigault, P. Böni, P. Coutois, A. Devishvili, N. Rebrova, M. Schneider, T. Soldner, Nucl. Instruments & Methods Phys. Res. A 840 (2016) 181–185.
[2] M. Janoschek, P. Böni, M. Braden, Nucl. Instruments & Methods Phys. Res. A 613 (2010) 119–126.
[3] A.C. Komarek, P. Böni, M. Braden, Nucl. Instruments & Methods Phys. Res. A 647 (2011) 63.
[4] D. Gorkov, P. Böni, M. Braden, 2024, submitted to Nuclear instruments & methods in physics research A, in process.
[5] J. Tanabe, Iron Dominated Electromagnets: Design, Fabrication, Assembly and Measaurements, World Scientific Publishing Company, 2005, ISBN: 10:9789812563811.
[6] G. Schnell, Magnete: Grundlagen, Aufbau, Anwendung, vol. 49, (1974) 1974, ISBN: 10:3521060829,
[7] SwissNeutronics AG, Bruehlstrasse 28, CH-5313 Klingnau, Switzerland, Polarization broschure, 2025, https://www.swissneutronics.ch/fileadmin/user_upload/Dokumente/Bilder/Products/Polarizing_Devices/Flyer_ESS_-_polarising_devices_-_V3.pdf. (Accessed 2025-05-06).

[8] M.D. Coey, Applications of hard magnets, in: Magnetism and Magnetic Materials, Cambridge University Press, Cambridge, 2010, pp. 464–493.
[9] S. Pasini, O. Holderer, T. Kozielewski, D. Richter, M. Monkenbusch, Rev. Sci. Instrum. 90 (2019) 043107.
[10] H. Soltner, U. Pabst, M. Butzek, M. Ohl, T. Kozielewski, M. Monkenbusch, D. Sokol, L. Maltin, E. Lindgren, S. Koch, D. Fugate, Nucl. Instrum. Methods Phys. Res. 644 (2011) 40–47.
[11] M. Monkenbusch, et al., 2024, in process.
[12] P. Blümler, H. Soltner, Appl. Magn. Reson. 54 (11) (2023) 1701–1739.
[13] K. Halbach, Proc. of the Eighth Int. Conf. on Rare Earth Magnet Materials, University of Dayton, Dayton OH, 1985, p. 123.
[14] H. Raich, P. Blümler, Concepts Magn. Reson. Part B (Magn. Reson. Eng.) 23B (2004) 16–25.
[15] H.A. Leupold, Permanent magnet design: Magnetic cladding and periodic structures, Magnetic Hysteresis in Novel Magnetic Materials, Springer, Netherlands, 1997, pp. 811–844.
[16] C.W. Windt, H. Soltner, D.van. Dusschoten, P. Blümler, J. Mag. Res. 208 (2011) 27–33.
[17] S. Russenschuck, Field Computation for Accelerator Magnets, Wiley-CVH Verlag GmbH & Co. KGaA, 2010.
[18] Metrolab, THM 1176 low-field hall Teslameter, www.metrolab.com.